AXIAL GAP OPTIMISATION OF HALF DIAMETER SHIFTED COUNTER ROTATING DUAL ROTOR WIND TURBINE

Csaba Hetyei[1], * and Ferenc Szlivka[2]

[1]Óbuda University, Doctoral School on Safety and Security Sciences
 Budapest, Hungary

[2]Óbuda University, Donát Bánki Faculty of Mechanical and Safety Engineering
 Budapest, Hungary

ABSTRACT

General energy demand is continuously increasing due to the fact that wind turbines and other renewable energy sources have begun to appear in previously unexplored areas, such as on the roofs of buildings. In view of this demand, a new type of wind turbines described in this article could become one of the energy generating tools in a smart grid system. In this article, first conventional and unconventional wind turbines are reviewed with respect to efficiency. Then a Counter Rotating Dual Rotor Wind Turbine (CO-DRWT) construction is analysed with Computational Fluid Dynamics (CFD) codes considering a fixed radial and a variable axial distance. In the analysis, power coefficients were calculated for different configurations. It was found that in case of the dual rotor wind turbine, the optimal axial distance for half diameter radial shift was in the range of 0,2-0,25 diameter.

KEY WORDS

CLASSIFICATION

*Corresponding author, η: hetyei.csaba@phd.uni-obuda.hu; +36 1 666 5449;
 Népszínház street 8., 1081 Budapest, Hungary

INTRODUCTION

Due to the increasing demand for energy, the extraction of renewable energy sources comes into focus increasingly frequently. Renewable energy has different sources depending on the potentials of the location.

By reviewing the global market of renewable energy sources, we can see a growing trend from year to year. By the study of Frankfurt School – UNEP Collaborating Centre for Climate & Sustainable Energy Finance [1] in 2018, the estimated new investment was 133,5 billion USD for solar, 129,7 billion USD for wind, 6,8 billion USD for waste energy technologies, such as biomass, 2 billion USD for geothermal, 481 million USD for biofuels, and 359 million USD for small hydro powers. The overall estimated new capacity installation cost was 272,9 billion USD, which is less by 12 % compared to the new investments in 2017. Researchers have been working on improving the power cycle efficiency in order to decrease the cost of renewable energy. For example, the use of supercritical CO_2 as working fluid in power cycles has the potential to revolutionise power generation [2].

In the urban area where usually a traditional energy system is available, several base power plant provides the electricity. In contrast to the traditional system, in the smart grid next to the base power plant there are variable energy sources, i.e. renewable energy sources. The strength of this system is that any small scale energy sources could be the main power plant for a sub-system for a required time interval. For example, for small electrical devices like a coffee machine PV panels or small scale wind turbines could complete the available big scale power plant's electric production.

Focusing solely on the wind energy sector, the first wind turbine (WT) was invented by James Blyth in 1887, which was a vertical axis wind turbine (VAWT). The first horizontal axis wind turbine (HAWT) was invented by Charles Brush and built in 1888. This two WTs are shown in Figure 1.
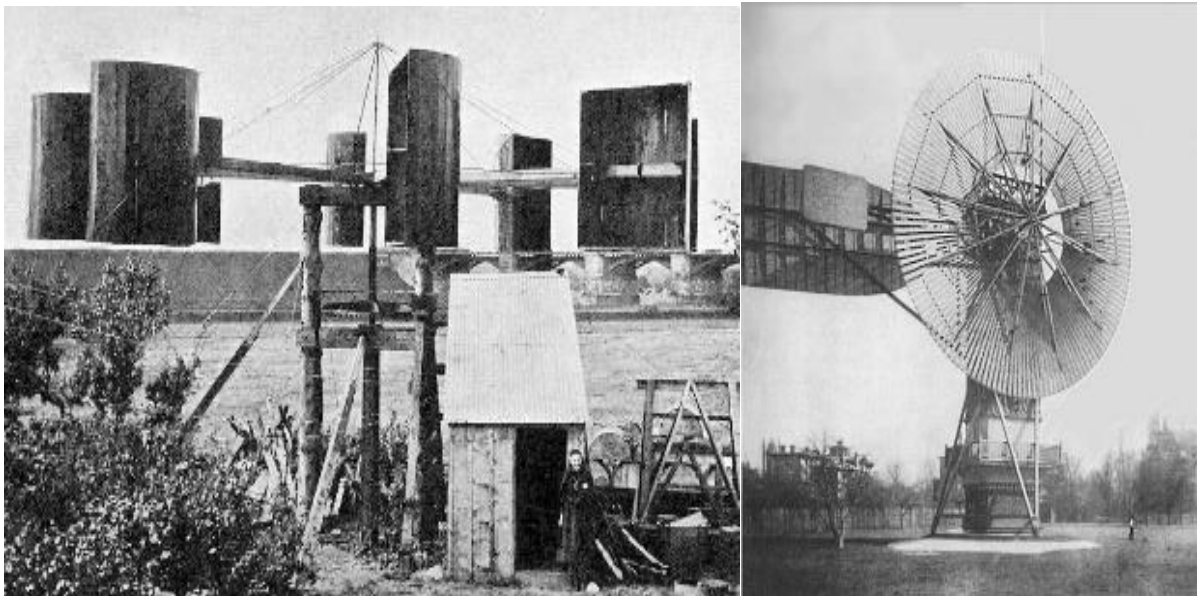

Figure 1. James Blyth's (left) and Charles F. Bush's (right) WT [3, 4].

While the first WT's structures were constructed of wood and canvas, nowadays turbines are constructed of steel, concrete, glass fiber and epoxy matrix composite materials. Thanks to these new materials and the growing demand for electricity, an increasing number of WTs appearing in the cityscape.

Figure 2. Wind turbines mounted on buildings. A) World Trade Center in Bahrain [5] b) Strata SE1 Tower [6].

Nowadays, due to the development and installation of a growing number of WTs, it is important to examine how multiple wind turbines in close proximity interact with each other and with the installation areas, such as buildings in the urban region. A. Nagy and I. Jahn [7]398 have shown a measurement system that is capable to measure flow parameters between wind turbines. The technology of WTs is evolving continuously to be more autonomous, sustainable and economical. Innovations helped in the development of new parts, e.g. guide baffles, new blade structures and profiles, some of which are shown in Figure 3.

Figure 3. Unconventional WTs. A) Guide baffle [8], b) Archimedes Screw Wind Turbine [9], c) Hi-Q wind turbine [10].

The layouts of multiple "standard" turbines used on the same tower may only be limited by imagination, as new structural innovations are being considered. There are different approaches when the turbines are installed on different axes or on the same rotating axis. For the latter type, depending on the rotating direction, the turbines are called co-rotating or counter-rotating dual rotor wind turbines (CR-DRWT and CO-DRWT). These unconventional WTs are shown in Figure 4.
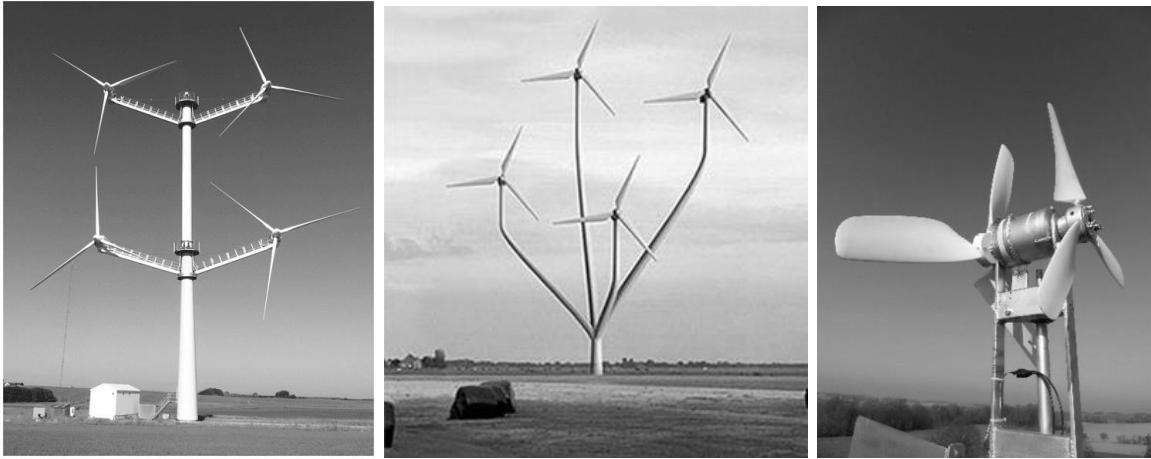

Figure 4. Unconventional twin and multi WTs [11-13].

Lee et al. [14] simulated a CO-DRWT's power coefficient, c_p by using the blade element momentum theory and they compared it with a c_p of a traditional single-rotor wind turbine (SRWT). As a result, the CO-DRWT showed in some cases higher performance for different pitch angle, rotating speed and radius ratio compared to the SRWT.

The power coefficient, c_p, which we were refed can be calculated with the following equation:

$$c_p = \frac{P_{rotor}}{P_{wind}} = \frac{M \cdot \omega}{\frac{1}{2} \rho \cdot A \cdot v_\infty^3} \tag{1}$$

In the equation, P_{rotor} is rotor's power, P_{wind} is the wind power, M is the torque, ω is the angular velocity, ρ is the density of the air, A is the swept area, v_∞ is the freestream velocity.

Ozbay et al. [15] performed an experimental study to compare the power production performance of CR and CO DRWTs compared to SRWTs. They found the DRWTs' overall c_p was higher than the SRWT's. Furthermore, they found that the counter-rotating DRWT can harvest more energy than the co-rotating DRWT.

Theoretically, c_p has a maximum value, which was calculated as 16/27 (59,26 %) by the one-dimensional Betz's law, and 30,113 % by the two-dimensional GGS model [16]. By the measurement results for the SRWT, the maximum efficiency was shown to be in between the GGS and the Betz limit.

MOTIVATION

In this research, a CO-DRWT was studied without the tower and a nacelle. In our analyses, the propeller layout was chosen as being fixed as 0,5D radially, and with a variable axial distance between 0,005 and 2D. (The D in the distance values represent the rotor diameter, which was 200 mm.)

For the initial position, the 180° shifting between the mirrored wheels "top" planes were selected to avoid overlapping between the blades. The initial geometry and the labelled distances are shown in Figure 5.
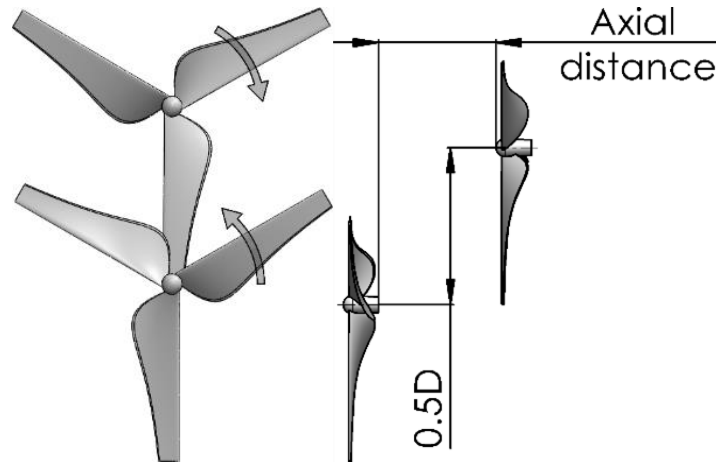

Figure 5. Studied counter-rotating dual rotor.

By numerical simulation, c_p values were calculated and compared for the studied cases.

SIMULATION AND EXPERIMENTAL METHODS AND SETTINGS

In the next subchapters, the finite volume method (FVM) is reviewed for the simulations, and our simulation's boundary conditions and measurement system are described.

SIMULATION METHOD

In the simulations, two different CFD (Computational Fluid Dynamics) software were used with the finite volume method.

The FVM divides the computational domain into finite volumes, and using the conservation laws (mass, momentum and energy) to compute the flow field properties. This calculation uses the transport equation of:

$$\frac{\partial}{\partial t} \int_V U \, dV = - \oint_A \underline{F} \, d\underline{A} + \int_V S_V \, dV + \oint_A \underline{S_A} \, d\underline{A} \tag{2}$$

In the equation, $\frac{\partial U}{\partial t}$ is the time-dependent member, U is a residual quantity's volumetric flux, F is the same residual's flux, S_V is the F flux's volumetric source, S_A is the F flux's surface source, V is the computational volume and A is the computational volume's surface.

The CFD codes solve this equation and its linked equations iteratively until the residual quantities do not decrease to a prescribed (near zero) value.

SIMULATION PARAMETERS

For the simulations, Mentor Graphics' FloEFD and Ansys CFX were employed.

In each simulation, we used air from the software's material database, which enters to the domain at the inlet face with 3,79 m·s^{-1} freestream velocity. The outlet faces had an environmental pressure of 1 atm, where the flow could quit from the domain. The wind turbine tip speed ratio was 4, which means the rotating region had 24,1279 RPS angular velocity.

For clarity, the tip speed ratio can be calculated by equation (3), where λ is the tip speed ratio, ω is the angular velocity, R is the blade's radius and v_∞ is the freestream velocity.

$$\lambda = \frac{\omega \cdot R}{v_\infty} \tag{3}$$

The simulation with FloEFD was in steady state with frozen rotor technique, and transient with the sliding mesh method. The unsteady simulation was run for 0,4144582 second, which is the time requirement for 10 rotations. In each state the k-ε turbulence model was used. In FloEFD, its own mesher was used, which provided a cartesian mesh with cell mating and cut-cell methods. For these simulations a rectangular computational domain was used (Figure 6).

For CFX, nearly the same boundary conditions were used as in FloEFD, with the following differences:

• for modelling the turbulence, the SST model was used,
• for meshing the body fitting and element sizing technique was used,
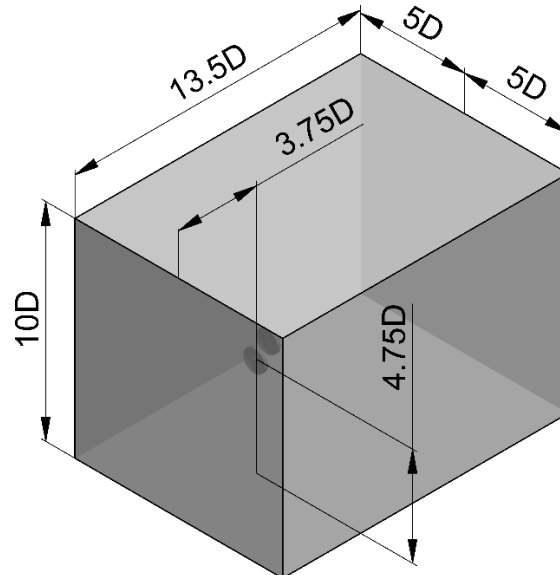• a tubular computational domain was used (Figure 7).

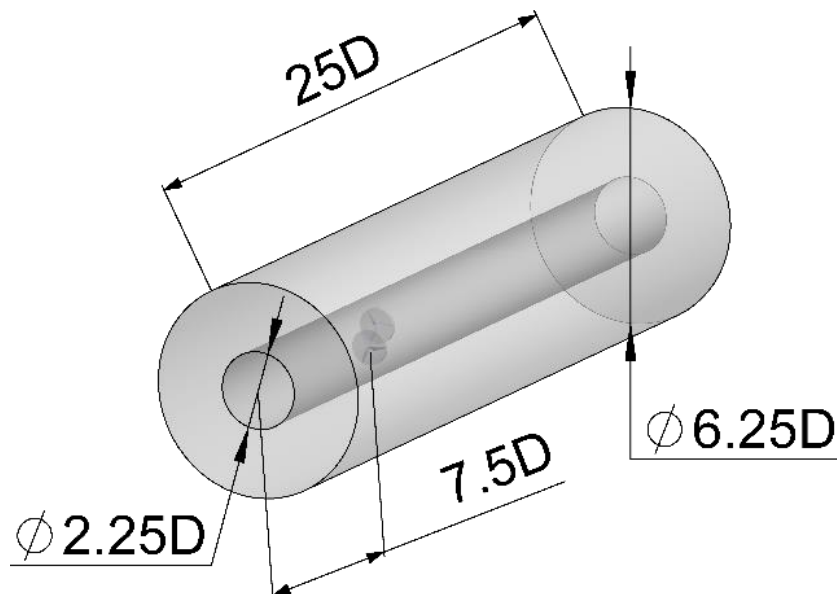**Figure 6.** Computational domain for FloEFD.

Figure 7. Computational domain for CFX.

Two different methods were used, the frozen rotor method (in steady state) for sweeping the whole axial range, and the sliding mesh technique (in unsteady state) for simulating the turbulence and checking the steady state result for the measured axial distance.

MEASUREMENT METHOD

For validating our simulation, a 3D printed version of the turbine wheels were used, which are shown in Figure 8.
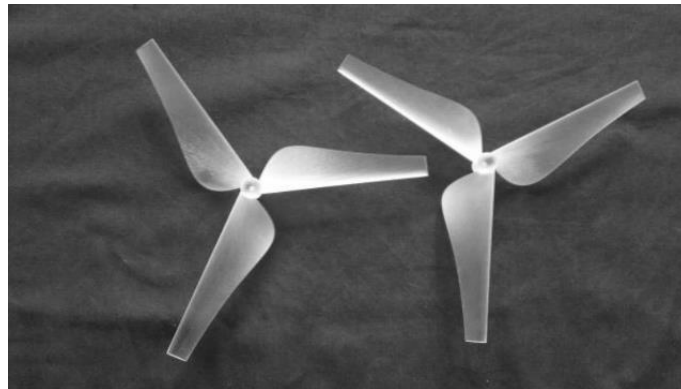

Figure 8. 3D printed wind turbine blades.

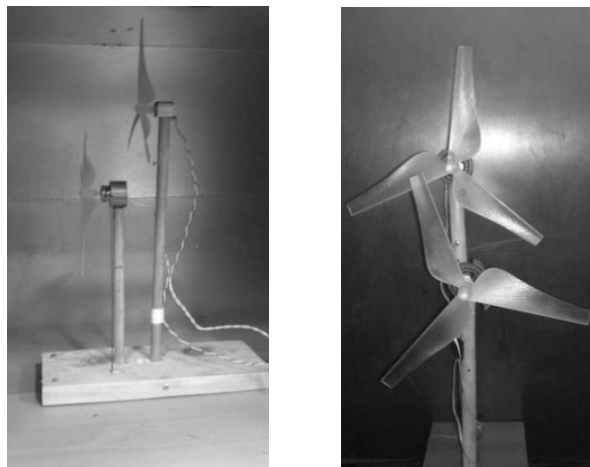The printed wheels were taken into a wind tunnel (Figure 9) where we were able to measure the generated torque [17].

Figure 9. Wind turbines in the wind tunnel.

RESULTS

In the software for each axial distance the flow field was similar. In the next figure (Figure 10) the velocity distribution near the turbines for A = 0,5D distance is shown.

Figure 10. Velocity field for $A = 0,5D$ distance, in unsteady state (zoomed).

For comparing our simulations, we were monitoring the torque on the surface of the blades. At the end of the simulation, in steady state the simulation affords a single value for the torque, while in transient the CFD software a torque value was produced for each time step. These time series are shown in Figure .
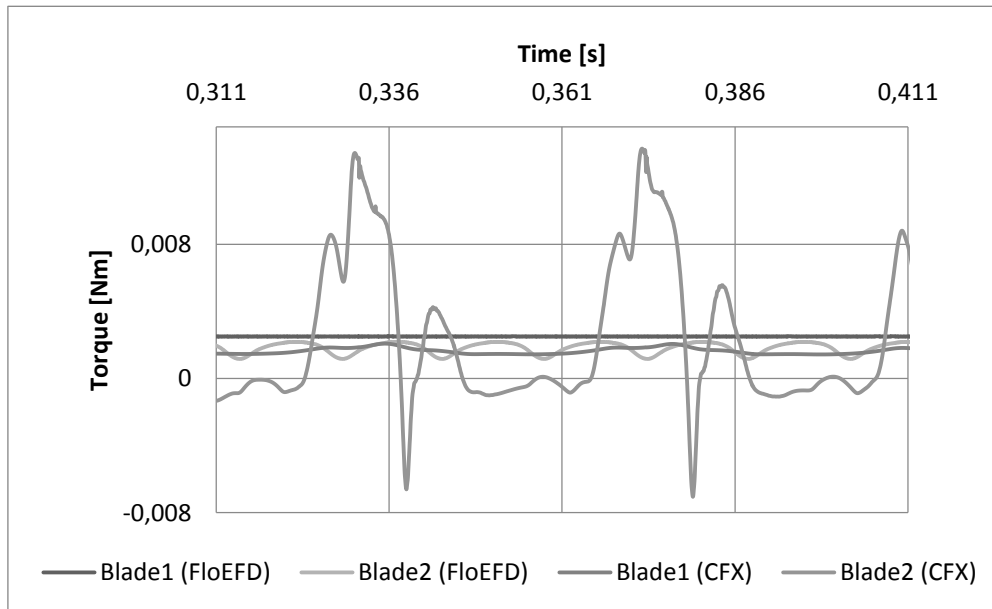

Figure 11. Torque values in the time domain.

The power coefficient (c_p) can be calculated from the torque and the boundary conditions. In Figure 12 the simulated c_p-s is shown, the frozen rotor technique (steady state) with blue dots, and the c_p with SST turbulent model in unsteady state (CFX) with the yellow square, and the c_p with k-ε turbulent model in unsteady state (FloEFD) with grey diamond, and the measured c_p with the red triangle. In each case, the c_p value is the sum of the two blades' power coefficients.
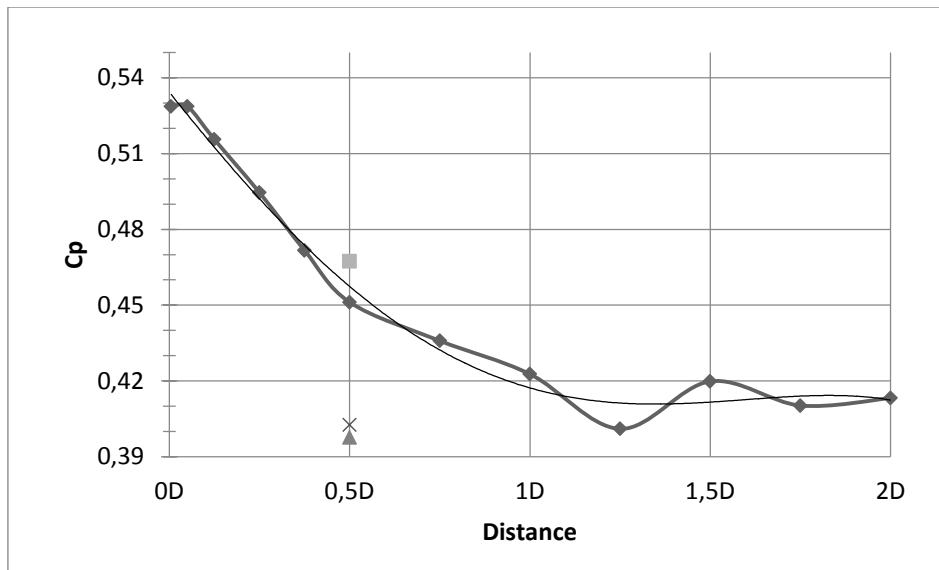
Figure 12. Power coefficient (c_p) versus the axial distance.

The simulated c_p with frozen rotor was 96,54 % while the simulated c_p with transient rotor stator was 86,15 % (with SST) and 86,08 % (with k-ε) of the measured c_p.

For comparison, we ran a simulation with frozen rotor technique for a one rotor turbine, and its power coefficient was 0,3424, which was 73,29 % of the measured CO-DRWT's c_p.

CONCLUSIONS

In this study, we were analysing a counter-rotating dual rotor wind turbine between 0,005D and 2D axial distance with a fixed 0,5D radial shift. At the end of the simulations, the power coefficient was plotted against the axial distance (Figure 11), and it was compared with a measured value.

Upon the results shown in Figure , the following statements can be established:

1) The power coefficient (c_p) was higher when the turbine wheels were closer.

2) In a built application, the zone before 0,2-0,25D was avoided, because the blade deformation could cause collisions.

3) The highest c_p was found at 0,05D. The second was at 0,005D, which is 0,01096 % smaller than value at A = 0,005D.

4) The dependence of the simulated c_p's with the distance can be modelled as $y = -0,0172 \cdot x^4 + 0,0487 \cdot x^3 + 0,0370 \cdot x^2 - 0,1792 \cdot x + 0,5343$ with the goodness of fit of $R^2 = 0,9874$.

5) The first wheel power coefficient (c_{p1}) and the second power coefficient (c_{p2}) were approximately the same in the 0,05-0,25D range.

6) After 1D axial distance, the c_{p1} value was 3 to 4 times larger than c_{p2}.

7) The SRWT's c_p value was 4,29 % larger than CO-DRWT's c_{p1} value for the 1.5D distance, 4,25 % more than the 1,75D's value and 3,01 % bigger than the 2D's value.

Upon conclusions 1) and 2), the recommended optimal distance was the closest where the blades do not have any collisions. For the required minimal distance, a measurement or a two-way FSI simulation is necessary.

We made the mesh dependency analysis for the A = 0,5D configuration, therefore, conclusion 3) might be a result of a numerical error. If not, the c_p of 0,05D has the largest value, therefore, it is energetically the best examined distance.

Regarding conclusion 7), we can establish that for large axial distance (like the 1,5-2D), a counter-rotating DRWT first rotor produces similar power like a single SRWT, therefore, the second rotor produces the extra power.

Based on the conclusions of the presented study, the CO-DRWT has a large potential as an engineering application for increased wind energy harvesting at small places where it is needed, such as in the urban areas of smart cities.

REFERENCES

[1] Frankfurt School-UNEP Centre: *Global Trends in Renewable Energy Investment 2019.*
https://wedocs.unep.org/bitstream/handle/20.500.11822/29752/GTR2019.pdf, accessed 20th September 2019,

[2] Braden, T., et al.: *The University of Queensland Refrigerant and Supercritical CO2 Test Loop.*
ASME Turbo Expo 2016: Turbomachinery Technical Conference and Exposition, Seoul, 2016,
http://dx.doi.org/10.1115/GT2016-58110,

[3] −: *James Blyth's Wind Turbine*.
https://upload.wikimedia.org/wikipedia/commons/1/13/James_Blyth%27s_1891_windmill.jpg, accessed 23rd September 2019,

[4] −: *Charles F. Brush Wind Turbine*.
https://media2.fdncms.com/clevescene/imager/tilting-at-windmills/u/zoom/2622441/cover-3.jpg, accessed 23rd September 2019,

[5] −: *World Trade Center in Bahrain.*
http://www.alternative-energy-news.info/images/pictures/wind-powered-towers.jpg, accessed 1st January 2019,

[6] −: *Strata SE1 Tower.*
https://upload.wikimedia.org/wikipedia/commons/d/d8/Strata_SE1_from_Monument_2014.jpg, accessed 1st January 2019,

[7] Nagy, A. and Jahn, I.: *Advanced Data Acquisition System for Wind Energy Applications.*
Periodica Polytechnica Transportation Engineering **47**(2), 124-130, 2019,
http://dx.doi.org/10.3311/PPtr.11515,

[8] −: *Unconventional Wind Turbines.*
http://www.whirlopedia.com/images/wind-turbines-elk.jpg, accessed 8th October 2019,

[9] −: *Bizarre Wind Turbines.*
https://cdn.trendhunterstatic.com/thumbs/urban-wind-turbine.jpeg, accessed 8th October 2019,

[10] −: *Hi Q Wind Turbine.*
https://www.darcorp.com/wp-content/uploads/2018/09/hi-q-wind-turbine-featuredLG.jpg, accessed 8th October 2019,

[11] Romańsk, L. et al.: *Estimation of operational parameters of the counter-rotating wind turbine with artificial neural networks*.
Archives of Civil and Mechanical Engineering **17**(4), 1019-1028, 2017,
http://dx.doi.org/10.1016/j.acme.2017.04.010,

[12] −: *Vestas Wind Turbine Tree.*
https://landartgenerator.org/blagi/wp-content/uploads/2016/04/191838856_b2b14fff9e_o.jpg, accessed 8th October 2019,

[13] Laan, M.P. et al.: *Power curve and wake analyses of the Vestas multi-rotor demonstrator.*
Wind Energy Science **4**(2), 251-271, 2019,
http://dx.doi.org/10.5194/wes-4-251-2019,

[14] Lee, S.; Kim, H.; Son, E. and Lee, S.: *Effects of design parameters on aerodynamic.*
Renewable Energy **42**, 140-144, 2012,
http://dx.doi.org/10.1016/j.renene.2011.08.046,

[15] Ozbay, A.; Tian, W. and Hu, H.: *Experimental Investigation on the Wake Characteristics and Aeromechanics of Dual-Rotor Wind Turbines.*
Journal of Engineering for Gas Turbines and Power **138**(4), 1-15, 2016,
http://dx.doi.org/10.1115/1.4031476,

[16] Gorban, A.N.; Gorlov, A.M. and Silantyev, V.M.: *Limits of the Turbine Efficiency for Free Fluid Flow.*
Journal of Energy Resources Technology, **123**(4), 311-317, 2001,
http://dx.doi.org/10.1115/1.1414137,

[17] Szlivka, F.; Molnár, I.; Kajtár, P. and Telekes, G.: *CFX Simulations by Twin Wind Turbine.*
2011 International Conference on Electrical and Control Engineering. IEEE, Yichang, 2011,
http://dx.doi.org/10.1109/ICECENG.2011.6057550.